JAAS

Accepted Manuscript

JAAS

Journal of Analytical Atomic Spectrometry
www.rsc.org/jaas

Volume 31 | Number 1 | January 2016 | Pages 1–346

Themed Issue: Celebrating the 30th Anniversary of JAAS

ISSN 0267-9477

ROYAL SOCIETY OF CHEMISTRY

CRITICAL REVIEW
Timur A. Labutin et al.
Femtosecond laser-induced breakdown spectroscopy

175 YEARS

This is an Accepted Manuscript, which has been through the Royal Society of Chemistry peer review process and has been accepted for publication.

Accepted Manuscripts are published online shortly after acceptance, before technical editing, formatting and proof reading. Using this free service, authors can make their results available to the community, in citable form, before we publish the edited article. We will replace this Accepted Manuscript with the edited and formatted Advance Article as soon as it is available.

You can find more information about Accepted Manuscripts in the **author guidelines**.

ROYAL SOCIETY OF CHEMISTRY

rsc.li/jaas

1

Detection and characterization of biogenic selenium nanoparticles in selenium-rich yeast by single particle ICPMS

3

4 Javier Jiménez-Lamana [a,*], Isabel Abad-Álvaro [b], Katarzyna Bierla [a], Francisco Laborda [b],

5 Joanna Szpunar [a], Ryszard Lobinski [a]

6

7 [a]Laboratoire de Chimie Analytique Bio-inorganique et Environnement (LCABIE), UMR 5254-

8 IPREM, CNRS-UPPA, Hélioparc, Pau, France

9 [b]Group of Analytical Spectroscopy and Sensors (GEAS), Institute of Environmental Sciences,

10 (IUCA) University of Zaragoza, Zaragoza, Spain

11

12 **Corresponding author**

13 *Telephone: +33540175037. E-mail: j.jimenez-lamana@univ-pau.fr

14

15 **ABSTRACT**

16 A method based on single particle inductively coupled plasma mass spectrometry (SP-ICPMS) was

17 developed for the analysis of commercial Se-rich yeasts, to confirm the occurrence of selenium

18 nanoparticles in these food supplements. A considerable reduction of the background levels was

19 achieved by combining data acquisition at microsecond dwell times and the use of H_2 reaction cell,

20 improving by a factor of 10 the current state-of-the-art methodology, and bringing size detection

21 limits down to 18 nm for selenium nanoparticles. The presence of nanoparticulate selenium was

22 unveiled by size-exclusion chromatography ICPMS, detecting a selenium peak at the exclusion

23 volume of the column showing absorption at the wavelength corresponding to selenium

24 nanoparticles. SP-ICPMS allowed to confirm the presence of Se-nanoparticles, as well as to

25 calculate the nanoparticle size distribution, owing to the information about the shape and elemental

26 composition of the nanoparticles obtained by transmission electron microscopy (TEM) and energy

27 dispersive X-ray spectroscopy (EDS), respectively. These results reveal the significance of

28 nanoparticles in the speciation of metals and metalloids in biological samples and the capability of

29 SP-ICPMS in combination with TEM-EDS to carry out these analyses.

30

31 1. Introduction

32 Tailored metal/metalloid biogenic nanoparticles with specific physiochemical properties have been

33 shown to be highly toxic to several pathogenic bacteria and may offer an attractive alternative for

34 therapy of infections by antibiotic resistant bacteria.[1,2] In particular, selenium nanoparticles (SeNPs)

35 synthesized by microorganisms, such as bacteria, fungi or yeast were demonstrated to possess

36 antibacterial, antiviral and antioxidant properties.[1,2] The process of the Se° nanoparticle formation is

37 based on the reduction of a toxic selenite (SeO_3^{2-}) or selenate (SeO_4^{2-}) to the less toxic (for the host

38 organism) elemental selenium through the intra- or extracellular formation of SeNPs with a typical

39 spherical shape and a diameter of 50-400 nm.[3,4]

40 Yeast is not only recognised as a model system to study selenite or selenate metabolic

41 detoxification pathways,[5] but it has also been the basis of an important biotechnological process of

42 their conversion to selenoamino acids, in particular to selenomethionine.[6] Indeed, yeast

2

43 (*Saccharomyces cerevisiae*) grown on selenite or selenate media, accumulates up to 3000 μg g^{-1} of

44 selenium, and has been used as a food and feed supplement,[6] and at high doses (>200 μg Se/day) in

45 prostate and colon cancer prevention treatments.[7] The subsequent authorizations obtained by several

46 companies for the commercialization of Se-rich yeast were preceded by the development of

47 analytical methods for the specific identification and quantification of the different chemical forms

48 of selenium present (speciation) of which the state-of-the art was reviewed.[8]

49 The currently available analytical methods allow the determination of selenomethionine

50 [with a relatively high confidence owing to the availability of a certified reference material (SELM-

51 1)],[9] selenocysteine and a water soluble metabolome fraction.[8] They also allow the determination of

52 the residual (non-reacted) selenite or selenate, referred to as "inorganic selenium" of which the

53 presence below 2% is considered by the legislators as a proof of an "organic" character of Se-rich

54 yeast.[10] Our experience over the past decade, through the analysis of several hundred samples from

55 about 20 different suppliers, indicates that the selenium mass balance for the identified species

56 rarely exceeds 90% which would suggest the presence of unaccounted forms of selenium.

57 To our best knowledge, Se° has never been quantified in yeast, although there were some

58 attempts to its quantification in garlic[11] and in *Thunbergia alata*[12] using operationally defined or

59 chemical conversion methods. Nanometer-sized deposits were reported in yeast cells grown in the

60 presence of selenium by using X-ray radiation fluorescence spectroscopy[13] without being

61 characterized more deeply or quantified. We are putting forward here a hypothesis that a certain

62 amount of selenium may be present in Se-rich yeast supplements as SeNPs and are proposing the

63 development of an analytical method for its verification.

64   To date SeNPs produced by microorganisms have been characterized by transmission

65   electron microscopy (TEM),[3,4,14-19] X-Ray diffraction (XRD)[20] and atomic force microscopy

66   (AFM).[19,20] For instance, TEM analyses provided evidence of the formation of electron-dense

67   granules in Se-treated microorganisms which were absent in the control ones.[3,4] The presence of

68   selenium in these granules could be confirmed by energy dispersive X-ray spectroscopy (EDS)

69   while the absence of peaks from other elements indicated the presence of Se in the elemental state

70   rather than as a selenide.[3,4] TEM was also applied for the characterization of SeNPs produced by

71   *Bacillus cereus*,[14] the soil bacterium *Pseudomonas putida* KT2440,[15] the filamentous bacterium

72   *Streptomyces sp.* ES2-5,[16] the rhizobacterium *Azospirillum brasilense,*[17,18] and a genetically

73   modified *Pichia pastoris* strain.[19] In the latter case, results were confirmed by AFM. On the other

74   hand, SeNPs of an average size of 21 nm produced by bacterial isolate *Pseudomonas aeruginosa*

75   strain JS-11 were characterized by XRD.[20] The morphology and size of the nanoparticles were

76   further validated by AFM. Recently, an alternative to TEM measurements was proposed by using

77   the capabilities of asymmetrical flow field-flow fractionation (AF4) coupled on- and off-line with

78   different detectors, such as diode array (DAD), dynamic light scattering (DLS) or inductively

79   coupled plasma mass spectrometry (ICP-MS)[21,22]. For example, biogenic SeNPs synthesized by

80   lactic acid bacteria (LAB) were characterized by AF4 coupled on-line with DLS and results in good

81   agreement with those obtained by TEM and nanoparticle tracking analysis (NTA) were obtained[22].

82   A major drawback of these methods is their difficulty to detect, characterize and quantify SeNPs at

83   low concentrations ($\mu g\ kg^{-1}$).

84   This limitation can be overcome by single particle inductively coupled plasma mass

85   spectrometry (SP-ICPMS), which is one of the emerging techniques for the detection,

4

86 characterization and quantification of nanoparticles.[23] The theoretical basis of SP-ICPMS was

87 outlined by Degueldre *et al*.[24] and further developed by Laborda *et al*.[25] SP-ICPMS is able to

88 discriminate (detect and quantify) dissolved versus particulate forms of the element in a sample, and

89 to provide information about the element mass content per particle. Moreover, if additional

90 information about their composition, shape and density is available, the size of the particles can be

91 obtained, as well as their number and mass concentration.[26]

92 The feasibility of SP-ICPMS is compromised by the achievable size detection limits. For

93 elemental selenium nanoparticles, a detection limit of 200 nm was estimated theoretically.[27] This is

94 by far too high for the microorganisms related applications, although this size detection limit was

95 calculated by using the low abundant (9.36%) ^{76}Se isotope, due to inherent problems for selenium

96 determination by ICPMS because of spectral interferences. This problem can usually be overcome

97 by using mathematical correction equations[28] or reaction/collision cells[29].

98 The objective of this work is the development of a method for the detection and size

99 characterization of selenium nanoparticles by single particle ICPMS with the aim to reduce

100 considerably the size-detection limits predicted up to now.[27] The method is going to be used to

101 verify the occurrence of inorganic nanoparticulate selenium in Se-rich yeasts, confirming the

102 hypothesis that this species must be included in the speciation schemes of this element in Se-rich

103 yeasts.

104

105 **2. Experimental**

106 **2.1. Standards, samples and reagents**

107   Diluted suspensions of gold and selenium nanoparticles were prepared from commercially available

108   materials. A reference gold nanoparticle suspension RM 8013 of 60-nm nominal diameter was

109   obtained from NIST (NIST, Gaithersburg, MD). Suspensions of selenium nanoparticles of nominal

110   diameters of 50 and 100 nm were purchased from Nanocs (Nanocs, New York, NY). Dilutions were

111   prepared in ultrapure water by accurately weighing ($\pm$ 0.1 mg) aliquots of the stock suspensions

112   after 1 min sonication (Branson 2510, Bransonic, Danbury, CT; nominal power and frequency: 100

113   W, 42 kHz +/- 6%). After dilution and before each analysis, the suspensions were bath sonicated for

114   1 min (same power and frequency). Longer sonication times were not used to avoid excessive

115   heating of the suspensions. Aqueous selenium solutions were prepared from a standard stock

116   solution of 10000 mg L^{-1} (Sigma-Aldrich, St. Louis, MO) by dilution in ultrapure water. Ultrapure

117   water (18.2 MΩ cm) was obtained from a Milli-Q system (Millipore, Guyancourt, France).

118   Selenium-rich Brewer's yeast samples (obtained from a commercial provider), corresponding to a

119   yeast strain *Saccharomyces cerevisiae*, grown in different concentrations of selenium were used.

120

121   **2.2. SP-ICPMS analysis and data processing**

122   An Agilent 7900 Inductively Coupled Plasma Mass Spectrometer (ICPMS) (Agilent, Tokyo, Japan)

123   was used throughout. The sample introduction system consisted of a concentric nebulizer and a

124   quartz cyclonic spray chamber. Default instrumental and data acquisition parameters are listed in

125   Table 1. Settling time during data acquisition was eliminated and the total acquisition time was 60 s

126   in all experiments.

127   Nebulization efficiency was calculated according to the particle frequency method

128   developed by Pace *et al.*[30] The sample flow rate was calculated daily by measuring the mass of

6

129   water taken up by the peristaltic pump for two minutes. This operation was repeated three times and

130   the average value used for calculations. Under the experimental conditions used along this work, the

131   nebulization efficiency at a sample flow rate of 0.35 mL min^{-1} was 3.5 %.

132   Dwell times of 5 ms and 100 μs were studied and isotopes ^{80}Se and ^{78}Se monitored. Single

133   Nanoparticle Application Module for ICPMS MassHunter software (Agilent), as well as in-house

134   developed programs based on MatLab (MathWorks, Natick, MA) and Excel (Microsoft, Redmond,

135   OR) spreadsheets were used for data processing. OriginPro 8 data analysis software (OriginLab

136   Corporation, Northampton, MA) was also used.

137

138   **Table 1** Default instrumental and data acquisition parameters for single particle ICPMS

Instrumental parameters	
RF Power	1550 W
Argon gas flow rate	
Plasma	15 L min^{-1}
Auxiliary	0.9 L min^{-1}
Nebulizer	1.10 L min^{-1}
Reaction cell flow rate (H$_2$)	5.0 mL min^{-1}
Sample uptake rate	0.35 mL min^{-1}
Data acquisition parameters	
Dwell time	5 ms, 100 μs
Readings per replicate	12000, 600000
Settling time	-
Total acquisition time	60 s
Isotopes monitored	^{78}Se, ^{80}Se, ^{197}Au

139

7

2.3. Size Exclusion chromatography – ICPMS

A Superdex Peptide 10/300 GL column (GE Healthcare, Pittsburgh, PA) was coupled to an Agilent

7700x ICPMS (Agilent) instrument. Chromatographic separations were performed by using a model

1200 series HPLC pump (Agilent) as a delivery system. The exit of the column was connected in

series to an UV-visible detector (Agilent) and the ICPMS instrument.

2.4. Transmission electron microscopy

Samples were prepared on holey carbon films on mesh copper grids. A few microliters of each

sample were dropped on the grid and left to dry completely. Images were obtained using a FEI

TECNAI 12 (FEI, Hillsboro, OR) and recorded using an ORIUS SC1000 11MPx (GATAN,

Pleasanton, CA) CCD camera. The microscope is equipped with an energy-dispersive X-ray

analysis system for elemental analysis.

2.5. Procedures

2.5.1. Acid digestion. The content of total selenium in selenium nanoparticle suspensions

and Se-rich yeast samples was determined by ICPMS following acid digestion in a DigiPREP

digestion system (SCP Science, Quebec, Canada). 250 μL of H_2O_2 (VWR International, Fontenay-

sous-Bois, France) and 1 mL of conc. HNO_3 (Baker, Deventer, Netherlands) were added to 250 μL

of sample. The digestion was performed at 65 °C for 4 h. After digestion the volume was made up

to 50 mL so that the final HNO_3 concentration was 2% (v/v). Digestions were made in duplicate.

Blanks were run in parallel with the samples, as well as Certified Reference Material SELM-1

161 (National Research Council of Canada) was analysed in order to validate the total selenium

162 determination after acid digestion.

163 **2.5.2. Enzymatic digestion.** The digestion/extraction procedure included four steps: (1) 200

164 mg of a Se-rich yeast sample were suspended in 5 mL of water, bath sonicated for 1 h and

165 centrifuged at 4500 x g for 10 min; (2) the pellet was resuspended with a solution of 5 mL of

166 driselase (Sigma Aldrich, Saint-Quentin Fallavier, France) 4% (*m/v*) in Tris (Sigma Aldrich) 30

167 mM at pH 7.5, incubated at 25°C for 17 h and centrifuged at 4500 x g for 10 min; (3) the pellet was

168 resuspended with a solution of 5 mL of protease (Sigma Aldrich) of 4 mg L^{-1} in Tris 30 mM at pH

169 7.5, incubated at 37°C for 17 h and centrifuged at 4500 x g for 10 min; (4) finally, the pellet was

170 resuspended with a solution of 5 mL of sodium dodecyl sulphate (SDS, Sigma Aldrich) of 4%

171 (*m/v*), bath sonicated for 1 h and centrifuged at 4500 x g for 10 min. The supernatant was recovered

172 and kept at 4°C until analysis. One of the samples was subjected to an extra step: 1 mL of the SDS

173 extract was digested with a 1 mL protease solution of 4 mg L^{-1} in Tris 30 mM at pH 7.5, incubated

174 at 37°C for 17 h and centrifuged at 4500 x g for 10 min.

175

176 3. Results and discussion

177 3.1. Selection of instrumental parameters for the improvement of size detection limits

178 In SP-ICPMS, the size detection limit is critically dependent on the detection efficiency (ions

179 arriving to the detector with respect to the atoms in the plasma) and the background signal. Isobaric

180 and matrix/plasma polyatomic interferences, as well as dissolved species of the element measured

181 contribute to the continuous baseline in the time scans recorded in single particle mode. The most

182 significant effect of a high baseline level is the loss of capability to identify particles with smaller

183 amounts of the element measured, and hence the increase in the size detection limits.[31]

184   Selenium has 6 naturally occurring stable isotopes with abundances from 0.9 to 49.6%

185 which are severely interfered mostly by Ar containing ions (Table S1). This problem has been

186 overcome in quadrupole ICPMS by selecting less-interfered isotopes (e.g., ^{82}Se) or by using

187 mathematical correction equations.[28] However, the use of reaction/collision cells[29] should allow the

188 use of the most abundant isotopes ^{80}Se and ^{78}Se,[32,33] which are otherwise severely interfered by Ar

189 dimers. The fact that the size detection limit value of 200 nm was estimated by Lee *et al.*[27] using

190 relatively-low abundant ^{76}Se (9.36%) suggests a large margin for improvement of the size detection

191 limit of SeNPs if a high abundance isotope is selected and the polyatomic interferences removed.

192 Finally, a decrease of dwell times from milliseconds to microseconds would result in a proportional

193 reduction of the absolute baseline level[34] and hence of the related noise. The above considerations

194 were the basis of the method optimization strategy.

195   **3.1.1. Choice of the isotope: effect of the collision cell.** Our goal was to use one of the two

196 most abundant selenium isotopes, ^{78}Se and ^{80}Se, by reducing or eliminating the background

197 interferences. Apart from the contribution of residual Kr in the Ar gas supply, the main plasma

198 background contributions at masses 78 and 80 arise from Ar dimers. Indeed, the direct measurement

199 at m/z 80 is not possible, as the background exceeds 6.4×10^7 cps (time scans are shown in Fig. S1);

200 a considerable background (4.1×10^4 cps) is also observed for ^{78}Se. The use of collision/reaction

201 cells to reduce argon-based polyatomic interferences has been previously reported in literature (but

202 never for selenium in the single-particle mode), with the use of different gases such as methane[35-37]

203 or a He-H$_2$ mixture.[32] For instance, the potentially interfering argon dimers at the selenium masses

10

204　74, 76, 78 and 80 were reduced by approximately five orders of magnitude by using methane as

205　reactive cell gas.[35] In our case, the pressurization of the collision cell with H_2 (5.00 mL min^{-1}) led to

206　a 5 x 10^3-fold decrease in the background for ^{78}Se (down to 8 cps) and 7 x 10^5-fold for ^{80}Se (down

207　to 90 cps). Therefore, the use of the reaction cell leads to an important decrease of background

208　signals in both cases, being more pronounced at mass 80. If sensitivities at mass 78 with and

209　without reaction cell are compared, an improvement of more than twice is observed using H_2, which

210　is explained through the isotopic abundance of the isotopes. Table 2 summarizes the background

211　signals, the standard deviation of the associated noise, the signal-to-noise ratio and the sensitivity

212　(slope of the calibration curve for selenium water solution) which allowed the calculation of the

213　attainable concentration detection limits for the different selenium isotopes in the standard and

214　collision/reaction cell modes.

215

216　**Table 2** Background signals, associated noise (expressed as standard deviation of background),

217　signal-to-noise ratio, sensitivity and attainable concentration detection limits for the different

218　selenium isotopes when measured with and without collision/reaction cell. Dwell time: 100 μs

| Se	H_2 cell	Background (cps)	Noise (cps)	Sensitivity (cps L μg^{-1})	S/N	LD (μg L^{-1})
80	No	63700000	2160000	O/R	---	---
78	No	41300	18800	7700	0.04	7.33
80	Yes	90	995	40600	40.8	0.074
78	Yes	8	300	17800	59.33	0.051

219

220　　**3.1.2. Dwell time.** When a sufficiently diluted suspension of nanoparticles is introduced

221　into the plasma, each particle produces an individual pack of ions which is detected as such. By

11

222 using dwell times in the millisecond range (3-10 ms), events corresponding to the detection of

223 single particles are detected as single pulses, whereas they are detected as transient signals when

224 microsecond dwell times (<100-200 μs) are selected. On the other hand, the dissolved species

225 present together with the residual plasma background, produce a constant signal in the detector. The

226 intensity of this signal, expressed in counts, decreases proportionally if dwell times are shortened[32]

227 whereas the corresponding noise diminishes according to the square root of the background (for

228 signals below ca. 1000 counts, shot noise being the main contribution to the noise).[26]

229   Fig. 1 compares the time scans at dwell times of 5 ms and 100 μs with reaction cell

230 recorded for water and for a 50-nm selenium nanoparticle suspension with a nanoparticle number

231 concentration of ~ 1.85 x 10^8 L^{-1}. When working in the milliseconds regime (Figs. 1a, c), an

232 averaged baseline signal of 3.4 counts was measured. However, when the dwell time was shortened

233 to 100 μs (Figs. 1b, d) the intensity of the baseline was close to zero. Therefore, working in the

234 microsecond range instead of the millisecond range, makes it possible to reduce the contribution of

235 the background and thus to improve the size detection limits.

236

237
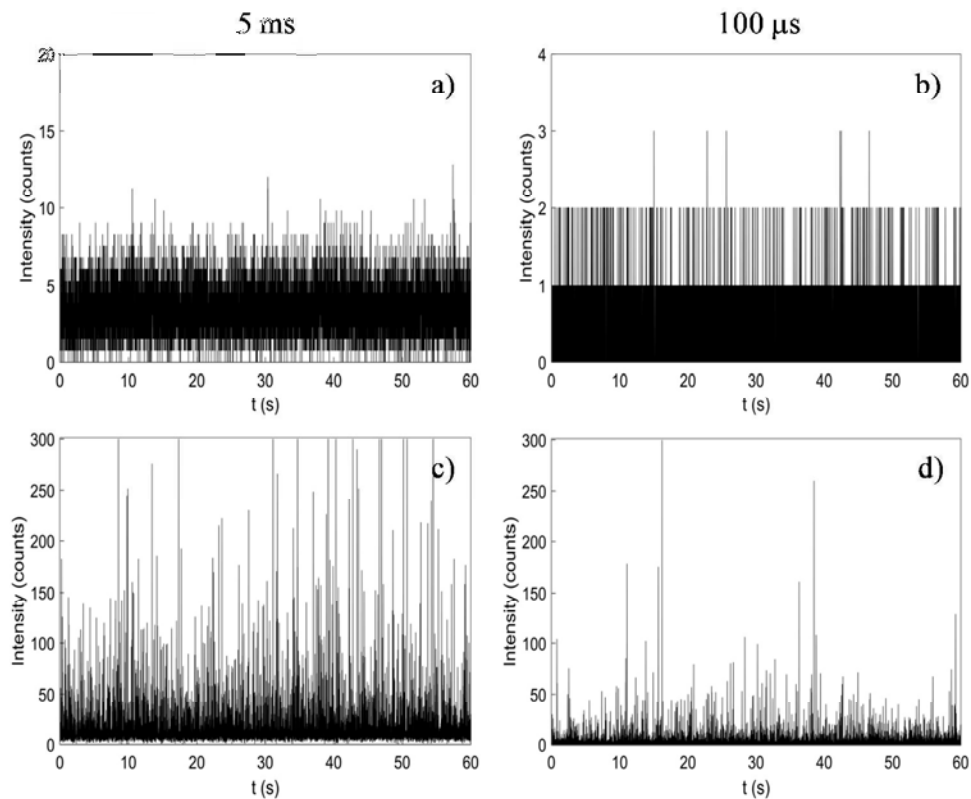
Fig. 1 ^{80}Se time scans of (a-b) ultrapure water, (c-d) 50-nm nanoparticle suspension of 1.85 x 10^{8} L^{-}
239 ^{1}. Dwell times: 5 ms, 100 μs.

240

3.2. Size detection limits

242 The intensity corresponding to the dissolved species or/and the background (μ_B) affects directly the

243 attainable size detection limit (LOD$_{size}$) through its standard deviation (σ_B). Applying a 3σ

244 criterion[25] for spherical, solid, and pure nanoparticles, and estimating σ$_B$ as the square root of the

245 background counts plus one[31], the LOD$_{size}$ is given by:

246

13

$$LOD_{size} = \left(\frac{18\,\sigma_B}{\pi\,\rho\,X_{NP}K_{ICPMS}K_M}\right)^{\frac{1}{3}} = \left(\frac{18\,\sqrt{\mu_B + 1}}{\pi\,\rho\,X_{NP}K_{ICPMS}K_M}\right)^{\frac{1}{3}} \qquad (1)$$

247

248   where ρ is the density of the nanoparticles, X_{NP} the mass fraction of the element in the nanoparticle,

249   K_{ICPMS} the detection efficiency (ratio of the number of ions detected versus the number of atoms

250   introduced into the ICP), and K_M ($=AN_{Av}/M_M$) includes the contribution from the element measured

251   (A, atomic abundance of the isotope considered; N_{Av}, Avogrado number; M_M, the atomic mass).

252   Apart from the influence of dissolved/background on LOD_{size}, Equation 1 includes the

253   detection efficiency, which depends on the particular instrument. On the other hand, the relationship

254   between the signal R (ions counted per time unit) and the mass concentration C^M of a solution of an

255   analyte nebulized into an ICPMS can be expressed as:

256

257
$$R = K_{intr}K_{ICPMS}K_M C^M \qquad (2)$$

258

259   where K_{intr} ($= \eta_{neb}\,Q_{sam}$) represents the contribution from the sample introduction system,

260   through the nebulization efficiency (η_{neb}) and the sample uptake rate (Q_{sam}), whose values are

261   detailed in section *2. Experimental*. By analysing a dissolved selenium standard and knowing the

262   value of K_{intr}, the term "$K_{ICPMS}\,K_M$" can be deduced from Equation 2.

263   Table 3 summarizes the LOD_{size} calculated for different selenium isotopes and dwell times

264   in water. By monitoring the most abundant isotope ^{80}Se, working with H_2 as reaction gas and with a

265   dwell time of 100 µs, a size detection limit of 18 nm could be achieved, considering: $\mu_B = 0.0092$

266   counts; $\rho = 4.79$ g cm^{-3}; $X_M = 1$; $\eta_{neb} = 0.035$; $Q_{sam} = 0.35$ mL min^{-1}; A = 0.4961; $N_{Av} = 6.022$ x

14

267   10^{23}; M_M = 78.96 g mol^{-1}; R/C^M = 40600 cps L µg^{-1}. Taking the above into account, monitoring ^{80}Se

268   and working in collision/reaction cell mode was concluded to be the best choice for the detection of

269   SeNPs by SP-ICPMS.

270

271   **Table 3** Size detection limits for selenium nanoparticles in water, nm

Dwell time	H$_2$ cell	^{78}Se, LOD$_{size}$	^{80}Se, LOD$_{size}$
5 ms	No	83	-
	Yes	25	24
100 µs	No	43	-
	Yes	24	18

272

273   **3.3. Analysis of commercial suspensions of selenium nanoparticles**

274   Two different commercial suspensions of SeNPs with nominal diameters of 50 and 100 nm were

275   analyzed by the developed method. Fig. 2 shows the time scans and the corresponding number size

276   distribution obtained for both commercial suspensions.

277

278
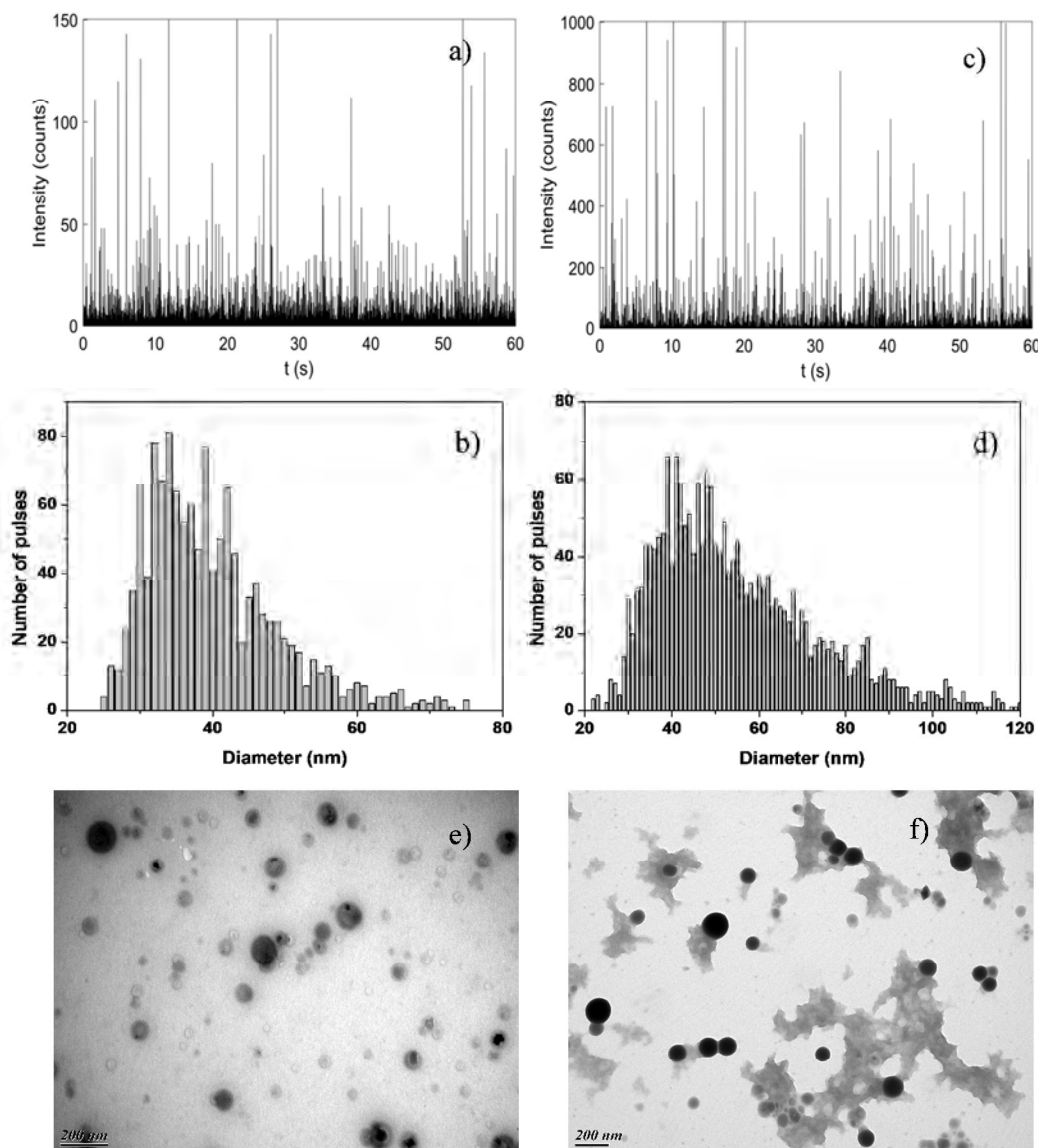
Fig. 2 ^{80}Se time scans of a) 50-nm Se nanoparticle suspension; c) 100-nm Se. Number size

distribution of b) 50-nm Se nanoparticle suspension; d) 100-nm Se. Dwell time: 100 μs.

Transmission electron microscope image of e) 50-nm Se nanoparticle suspension; f) 100-nm Se.

Scale bar: 200 nm.

283

284   The developed method allowed the detection of SeNPs as small as 20 nm in diameter. The

285   distributions showed an average diameter of 40.2 ± 0.4 nm for the nominal 50-nm particles and of

286   57.1 ± 0.1 nm for the nominal 100-nm particles. TEM images for both suspensions are presented in

287   Fig. 2e and 2f, showing spherical particles with no significant aggregation/agglomeration and some

288   polydispersity. The corresponding size distributions have been included in Fig. S2, showing that the

289   average sizes are in agreement with the nominal values (60 and 101 nm, respectively).

290   The disagreement between TEM and SP-ICPMS results can be explained by a different

291   response of the ICPMS towards the dissolved and the nanoparticulate selenium forms. To prove this

292   hypothesis, the total content of selenium in the commercial suspensions of SeNPs was determined

293   both by direct analysis of the diluted suspensions, and after their acid digestion. The calibration was

294   achieved with aqueous standards of selenium in water and 2% HNO_3 respectively, since a

295   dependence of the medium on the selenium sensitivity was observed. In order to verify the

296   completeness of the digestion procedure, the corresponding digested solutions were also measured

297   in single particle mode. No nanoparticle signals were observed, confirming that all the selenium

298   present was in its dissolved form or as particles below 18 nm. The concentrations determined in

299   water for the 50-nm and 100-nm SeNPs suspensions were 81.0 ± 3.4 % and 66.1 ± 7.6 % with

300   regard to the concentration determined after acid digestion, respectively (Table 4). These results

301   show that ICPMS sensitivity is dependent on the physicochemical form of selenium and on the size

302   of the nanoparticles. If nebulization efficiency is considered equal for dissolved and particulated

303   forms of selenium, the differences arises from the detection efficiency, most probably the less

304   efficient atomization or ionization of selenium nanoparticles.

305

17

306 **Table 4** Determination of selenium concentration in commercial suspensions of SeNPs in mg L^{-1}

307 (mean ± standard deviation)

Sample	50-nm	100-nm
Acid digestion	148.6 ± 5.5	92.1 ± 1.20
Suspensions in water	120.3 ± 2.2	60.85 ± 6.93

308

309

310   The different behaviour observed for the dissolved and nanoparticulate forms of selenium

311 implies that the use of dissolved selenium standards for calculations of the selenium mass per

312 particle or the size of a selenium particle will produce a negative bias and hence SeNPs with similar

313 selenium content or size of the targets should be used as standards.

314

315 **3.4. Detection and characterization of biogenic selenium nanoparticles in Se-rich yeast**

316 **samples**

317 The developed method was applied for the detection and characterization of putative selenium

318 nanoparticles present in selenium enriched yeast.

319   **3.4.1. Enzymatic digestion of the yeast matrix.** Yeast samples were submitted to an

320 enzymatic digestion prior to their injection onto a size exclusion column for the separation of the

321 selenium-binding species as explained in section *2. Experimental*. The effect of the digestion

322 procedure on the stability of SeNPs (dissolution or agglomeration) was also checked. For this, a Se-

323 free yeast sample was spiked with 100-nm SeNPs, submitted to the enzymatic digestion and

324 analyzed by SP-ICPMS. The size distribution obtained is shown in Fig. 3. In comparison with the

325 size distribution obtained for the original suspension (Fig. 2d), the size range was in good

18

326 agreement, proving that no agglomeration process occurred. However, obtaining the full

327 distribution was hampered by the presence of a relatively high background level, suggesting the

328 presence of dissolved selenium due to the partial oxidation of the nanoparticles.

329
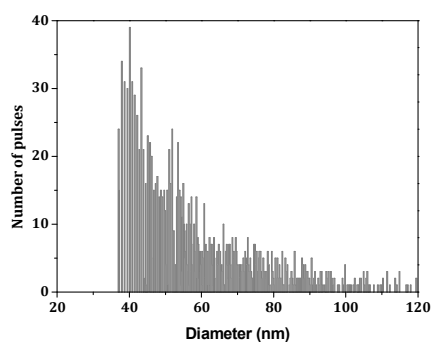
330 **Fig. 3** Number size distribution of 100-nm SeNPs suspensions after the enzymatic procedure.

331

332 **3.4.2. Detection of selenium nanoparticles in yeast.** The chromatograms obtained for a

333 Se-rich yeast sample by size exclusion chromatography with Visible and ICPMS detection are

334 shown in Fig. 4. Low molecular weight species were eluted as a single peak at 28 minutes, whereas

335 another selenium containing peak was observed at the exclusion volume of the column (10 min).

336 Only the peak at the exclusion volume also showed absorption at 565 nm, a wavelength associated

337 to SeNPs,[20,38] what suggests the presence of naturally occurring selenium nanoparticles in the yeast

338 sample.

339 Furthermore, the sample of yeast after the digestion procedure (Sample A) and the collected

340 fraction corresponding to the exclusion volume in the chromatogram (Sample A post column) were

341 analysed by SP-ICPMS under the previously optimized conditions (monitoring ^{80}Se, with H_2

19

342 reaction cell, dwell time: 100 µs). The time scans obtained showed a significant number of signals

343 above the background related to the presence of selenium-bearing nanoparticles in both cases (Figs.

344 5a, c). These time scans were transformed into signals distributions (Fig. S3). A different Se-rich

345 yeast sample (Sample B) was submitted to the same procedure and analysed by SP-ICPMS. In this

346 case, only a few signals above the background were observed (Fig. 5e), meaning the presence of a

347 small amount of selenium-bearing nanoparticles. This difference may be explained by the different

348 total concentration values in the original samples. The original yeast of sample A contained 3000

349 mg kg^{-1} while the total selenium concentration in the original yeast of sample B was 2000 mg kg^{-1}.

350 On the other hand, and in order to evaluate the particle detection capabilities of the method in real

351 samples, the size detection limits of the different samples were calculated by using the background

352 signal obtained in the time scans, obtaining values of 23, 20 and 19 nm for Sample A, Sample A

353 post column and Sample B, respectively.

354
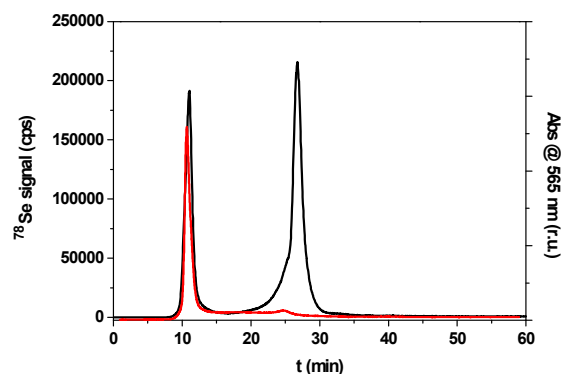
355

356 **Fig. 4** Chromatograms of a selenium enriched yeast sample after the digestion procedure, obtained

357 by ^{78}Se signal (black signal) and Vis signal recorded at 565 nm (red line). The first peak

358 corresponds to the void volume of the column.

20

359

360
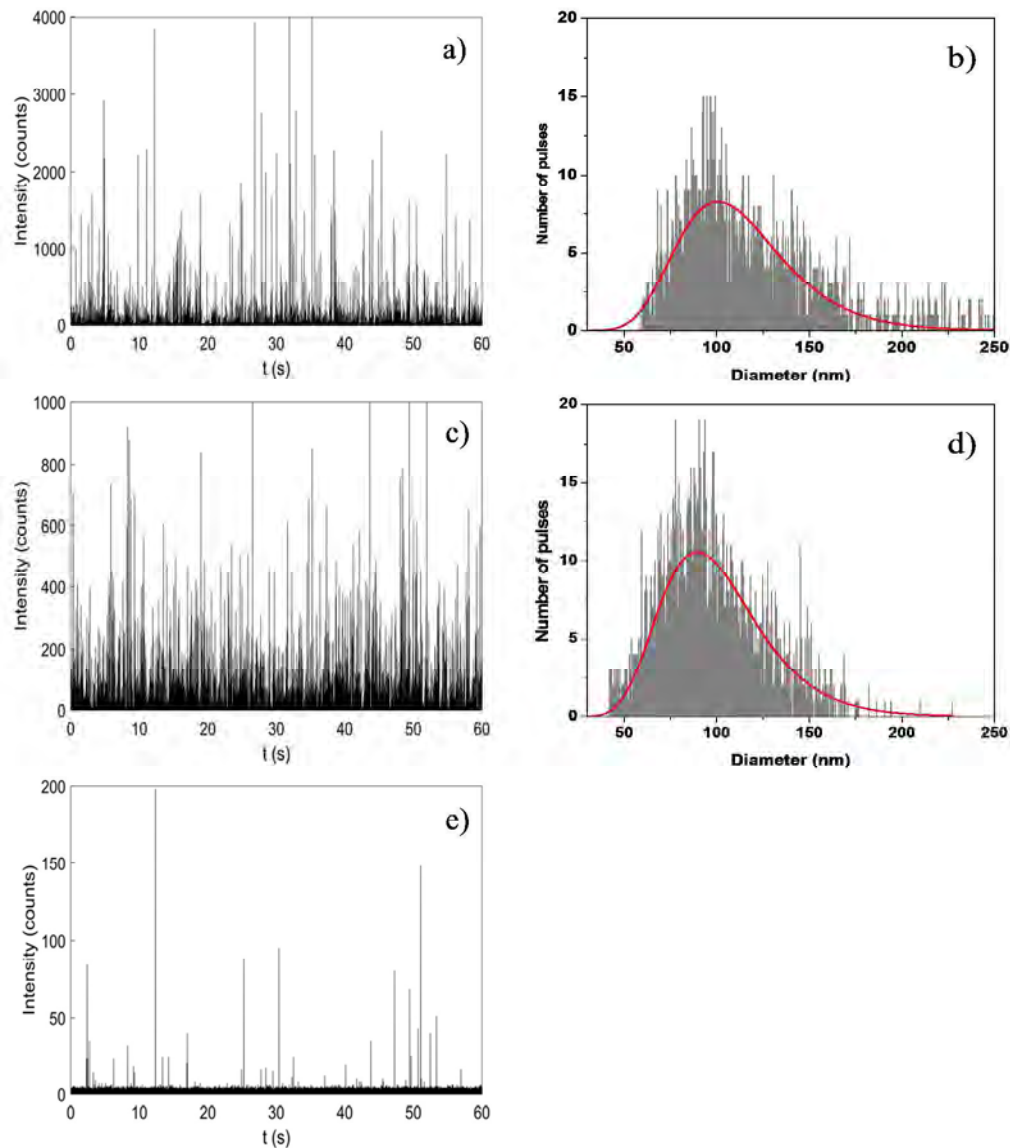
Fig. 5 [80]Se time scans and number size distributions obtained by SP-ICPMS corresponding to a-b)

Sample A; c-d) Sample A post column; and time scan corresponding to e) Sample B.

363

21

3.4.3. Size distribution of selenium nanoparticles. SP-ICPMS provides information about the mass of element per nanoparticle, which means that the conversion into size involves knowing the actual composition, density and shape of the nanoparticles. Additional techniques like transmission electron microscopy (TEM) and energy dispersive X-ray spectroscopy (EDS) were used to learn the shape and the elemental composition of the nanoparticles present in sample A. TEM images and EDS spectra obtained confirmed the presence of spherical nanoparticles whose composition was associated to elemental selenium (Fig. S4). Note that due to the low concentration of SeNPs in the sample, the number of particles detected in the images was too low to obtain a representative histogram, although a diameter around 100 nm could be measured from single images.

Once the composition and the shape of the nanoparticles were determined, the time scans were transformed into size distributions (Figs. 5b, d), using the density of bulk elemental selenium (4.79 g cm^{-3}). Due to the different behaviour in the ICPMS with respect to the size and the physicochemical forms of selenium, as previously discussed, and to the size of nanoparticles observed by TEM (~ 100 nm), a sensitivity correction factor of 66 % was applied on the mass of selenium per nanoparticle, calculated by using aqueous standards of selenium in water. The size histogram obtained for Sample A showed a broad distribution of selenium nanoparticles, from 60 to 200 nm (Fig. 5b). The size distribution was fitted into a log normal distribution and the median diameter was calculated, obtaining an average median diameter (n=5) of 108 ± 4 nm (average ± standard deviation). On the other hand, a similar size distribution was obtained for the fraction collected at the exclusion volume of the column (Sample A post column, Fig. 5d), with an average median diameter of 97 ± 3 nm (average ± standard deviation). These results are in good agreement

386   with the data from TEM, where nanoparticles around 100 nm were observed and confirmed that a

387   process of biosynthesis of selenium nanoparticles occurred in selenium enriched yeast.

388

389   **4. Conclusions**

390   An analytical method based on SP-ICPMS was developed for the detection and characterization of

391   SeNPs. The carefully optimization of parameters, including the monitored isotope, the choice of the

392   microsecond dwell time regime and the use of collision/reaction cell, allowed the reduction of the

393   background signal for using the most sensitive isotope of selenium. Under the optimal conditions, a

394   size detection limit of 18 nm could be obtained, which represents a gain of a factor of 10 in terms of

395   the prediction made elsewhere and the first ever single particle-ICP MS method for selenium

396   nanoparticle analysis. The method demonstrated the presence of SeNPs with sizes from 40 to 200

397   nm in Se-rich yeast and is able to provide information about the presence and size distributions of

398   nanoparticles at actual concentrations.

399

400   **Conflicts of interest**

401   There are no conflicts to declare.

402

403   **Supplementary Information**

404   Electronic supplementary information (ESI) available: Information about isotopic abundance and

405   spectral interferences for Se isotopes, time scans of ultrapure water, size distributions of SeNPs

406   suspensions, signal distributions of samples, TEM image and EDS spectrum.

407

414

References

416 1. M. Shakibaie, H. Forootanfar, Y. Golkari, T. Mohammadi-Khorsand, and M. R. Shakibaie, *J.*

417 *Trace Elem. Med. Biol.*, 2015, **29**, 235–241.

418 2. E. Cremonini, E. Zonaro, M. Donini, S. Lampis, M. Boaretti, S. Dusi, P. Melotti, M. M. Lleo,

419 and G. Vallini, *Microb. Biotechnol.*, 2016, **9**, 758–771.

420 3. S. Lampis, E. Zonaro, C. Bertolini, P. Bernardi, C. S. Butler, and G. Vallini, *Microb. Cell Fact.*,

421 2014, **13**, 35.

422 4. S. Lampis, E. Zonaro, C. Bertolini, D. Cecconi, F. Monti, M. Micaroni, R.J. Turner, C.S. Butler,

423 and G. Vallini, *J. Hazard. Mater.*, 2017, **324**, 3–14.

424 5. E. Herrero and R. Wellinger, *Microb. Cell*, 2015, **2**, 139–149.

425 6. G. N. Schrauzer, *Pure Appl. Chem.*, 2006, **78**, 105–109.

426 7. M. P. Rayman, *Br. J. Nutr.*, 2004, **92**, 557.

24

427   8. K. Bierla, J. Szpunar, A. Yiannikouris, and R. Lobinski, *TrAC - Trends Anal. Chem.*, 2012, **41**,

428   122–132.

429   9. H. Goenaga-Infante, R. Sturgeon, J. Turner, R. Hearn, M. Sargent, P. Maxwell, L. Yang, A.

430   Barzev, Z. Pedrero, C. Cámara, V. Díaz Huerta, M. L. Fernández Sánchez, A. Sanz-Medel, K.

431   Emese, P. Fodor, W. Wolf, R. Goldschmidt, V. Vacchina, J. Szpunar, L. Valiente, R. Huertas, G.

432   Labarraque, C. Davis, R. Zeisler, G. Turk, E. Rizzio, L. G. MacKay, R. B. Myors, D. L. Saxby,

433   S. Askew, W. Chao, and W. Jun, *Anal. Bioanal. Chem.*, 2008, **390**, 629–642.

434   10. European Food Safety Authority, *EFSA J.*, 2008, **766**, 1–42.

435   11. S. Mounicou, M. Dernovics, K. Bierla, and J. Szpunar, *Talanta*, 2009, **77**, 1877–1882.

436   12. F. A. Aborode, A. Raab, S. Foster, E. Lombi, W. Maher, E. M. Kruppa, and J. Feldmann,

437   *Metallomics*, 2015, **7**, 1056–1066.

438   13. Z. Mester, *European Symposium on Atomic Spectrometry ESAS,* 2014.

439   14. S. Dhanjal and S. S. Cameotra, *Microb. Cell Fact.*, 2010, **9**, 52.

440   15. R. Avendaño, N. Chaves, P. Fuentes, E. Sánchez, J. I. Jiménez, and M. Chavarría, *Sci. Rep.*,

441   2016, **6**, 37155.

442   16. Y. Tan, R. Yao, R. Wang, D. Wang, G. Wang, and S. Zheng, *Microb. Cell Fact.*, 2016, **15**, 157.

443   17. A. V. Tugarova, E. P. Vetchinkina, E. A. Loshchinina, A. M. Burov, V. E. Nikitina, and A. A.

444   Kamnev, *Microb. Ecol.*, 2014, **68**, 495–503.

445   18. A. A. Kamnev, P. V. Mamchenkova, Y. A. Dyatlova, and A. V. Tugarova, *J. Mol. Struct.*, 2017,

446   **1140**, 106–112.

447   19. F. Elahian, S. Reiisi, A. Shahidi, and S. A. Mirzaei, *Nanomedicine Nanotechnology, Biol. Med.*,

448   2017, **13**, 853–861.

25

Journal of Analytical Atomic Spectrometry Accepted Manuscript

449   20. S. Dwivedi, A. A. AlKhedhairy, M. Ahamed, and J. Musarrat, *PLoS One*, 2013, **8**, 1–10.

450   21. M. Palomo-Siguero, P. Vera, Y. Echegoyen, C. Nerin, C. Cámara and Y. Madrid, *Spectrochim.*

451   *Acta Part B J.*, 2017, **132**, 19–25.

452   22. G. Moreno-Martin, M. Pescuma, T. Pérez-Corona, F. Mozzi and Y. Madrid, *Anal. Chim. Acta*,

453   2017, **992**, 34–41.

454   23. F. Laborda, E. Bolea, and J. Jiménez-Lamana, *Trends Environ. Anal. Chem.*, 2016, **9**, 15–23.

455   24. C. Degueldre and P. Y. Favarger, *Colloids Surfaces A Physicochem. Eng. Asp.*, 2003, **217**, 137–

456   142.

457   25. F. Laborda, E. Bolea, and J. Jiménez-Lamana, *Anal. Chem.*, 2014, **86**, 2270–2278.

458   26. F. Laborda, J. Jiménez-Lamana, E. Bolea, and J. R. Castillo, *J. Anal. At. Spectrom.*, 2011, **26**,

459   1362.

460   27. S. Lee, X. Bi, R. B. Reed, J. F. Ranville, P. Herckes, and P. Westerhoff, *Environ. Sci. Technol.*,

461   2014, **48**, 10291–10300.

462   28. J. Goossens, L. Moens, and R. Dams, *Talanta*, 1994, **41**, 187–93.

463   29. S. D. Tanner, V. I. Baranov, and D. R. Bandura, *Spectrochim. Acta - Part B At. Spectrosc.*, 2002,

464   **57**, 1361–1452.

465   30. H. E. Pace, N. J. Rogers, C. Jarolimek, V. A. Coleman, C. P. Higgins, and J. F. Ranville, *Anal.*

466   *Chem.*, 2012, **84**, 4633.

467   31. F. Laborda, J. Jiménez-Lamana, E. Bolea, and J. R. Castillo, *J. Anal. At. Spectrom.*, 2013, **28**,

468   1220–1232.

469   32. I. Feldmann, N. Jakubowski, C. Thomas, and D. Stuewer, *Fresenius. J. Anal. Chem.*, 1999, **365**,

470   422–428.

471   33. J. M. Marchante-Gayon, C. Thomas, I. Feldmann, and N. Jakubowski, *J. Anal. At. Spectrom.*,

472   2000, **15**, 1093–1102.

473   34. I. Abad-Álvaro, E. Peña-Vázquez, E. Bolea, P. Bermejo-Barrera, J. R. Castillo, and F. Laborda,

474   *Anal. Bioanal. Chem.*, 2016, **408**, 5089–5097.

475   35. J. J. Sloth and E. H. Larsen, *J. Anal. At. Spectrom.*, 2000, **15**, 669–672.

476   36. U. Völkopf, K. Klemm, and M. Pfluger, *At. Spectrosc.*, 1999, **20**, 53–59.

477   37. S. D. Tanner, V. I. Baranov, and U. Vollkopf, *J. Am. Soc. Mass Spectrom.*, 2000, **15**, 1261–

478   1269.

479   38. Z. H. Lin and C. R. C. Wang, *Mater. Chem. Phys.*, 2005, **92**, 591–594.

480